ACS APPLIED OPTICAL MATERIALS

pubs.acs.org/acsaom

Forum Article

Electron Paramagnetic Resonance: A Technique to Locate the Nearest Environment of Chromium Luminescent Centers

Grzegorz Leniec*

Cite This: https://doi.org/10.1021/acsaom.3c00018

Read Online

ACCESS | Metrics & More | Article Recommendations

ABSTRACT: Electron paramagnetic resonance (EPR) magnetic studies make it possible to determine the nearest environment of luminescent ions if the ions are paramagnetic ones. It is the only research technique that directly determines the nearest environment of a doped (luminescent) ion. This article presents the most important magnetic analyses that should be performed for magnetic studies of luminescent ions. EPR studies make it possible to determine the types of luminescent centers, the point symmetry of these centers, and the distortion of the nearest environment of the luminescent centers. Temperature EPR and static magnetic susceptibility studies make it possible to determine the interactions between magnetic (luminescent) ions, the valence, and the concentration of these ions in the luminescent material. All these elements of magnetic investigations influence the position, shape, and efficiency of the luminescence spectrum.

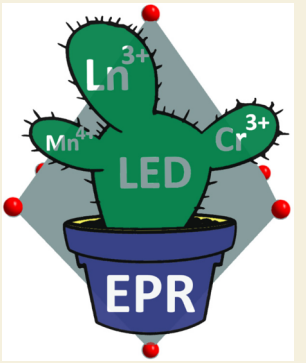

KEYWORDS: *electron paramagnetic resonance, electron spin resonance, paramagnetic ions, local symmetry, nearest environment, luminescence ions, chromium ions, Cr^{3+}*

INTRODUCTIONS

Luminescent ions are those whose energy levels allow them to emit radiation in the infrared, visible light, and ultraviolet ranges. These ions include rare earth (RE) ions (e.g., Ce^{3+}, Nd^{3+}, Eu^{3+}, Eu^{2+}, Dy^{3+}, Er^{3+}, Yb^{3+})[1−15] and transition metal ions (e.g., $Mn^{2+/3+/4+}$, Cr^{3+}, Ni^{2+}).[16−32] Due to the high cost of RE ions, transition metal ions are increasingly used. Transition metal ions most often occupy octahedral or tetrahedral sites depending on the valency of these ions. The range of radiation depends on the nearest environment of the luminescent ions. Mn^{2+} ions emit in the green color range, $Mn^{3+/4+}$ in the red color range, and Cr^{3+} ions in the infrared range. The shape and efficiency of the luminescence spectrum depend on the crystal environment of the luminescent ion. These include the crystal field (electric and magnetic), the point symmetry of the luminescent ion, the symmetry distortion of the nearest environment of the luminescent ion, Schottky/Frenkel defects in the vicinity of the luminescent ion, and the first and second coordination spheres. The first of the above issues can be determined from optical investigations, but the next is no less important only from electron paramagnetic resonance (EPR) studies. It should be noted that analyses of the nearest environment of luminescent ions by other research methods appear in scientific papers. However, dopants with a low concentration of luminescent ions can only be investigated using the EPR technique. This method is based on signal resonance and even more small magnetic ion quantities in the material can be investigated. Other studies investigate the nearest environment of ions in host materials and, assuming similar ion radii, luminescent ions are assumed to have the same symmetry as host material ions. However, this is only an assumption and not a result of the experiments that it can derive from the EPR method. In scientific papers on luminescence, EPR spectra are presented to verify the valence of ions and determine the symmetry of the nearest environment of luminescent ions. Usually these are single EPR spectra at room temperature. For luminescent chromium ions, the analysis involves determining the position of the EPR line relative to the magnetic induction, that is, determining the g_{eff} value. If the main EPR line (with the highest intensity) is located at low magnetic inductions ($g_{eff} > 3$), it means that the signal originates from single Cr^{3+} ions in an octahedral environment. However, for low symmetries and distortions, additional EPR lines appear, of which only the one at $g_{eff} \sim 2$ is interpreted. Regardless of the width and intensity of the EPR line, it is assumed that it originates from Cr^{3+}−Cr^{3+} pair interactions, even when optical studies do not reveal luminescence from Cr^{3+}−Cr^{3+} ion pairs. In the paper by Zhenwei Jia et al.[33] the authors increase internal quantum efficiency (IQE) by adding fluxes and sintering in a reducing atmosphere $Ca_3Sc_2Si_3O_{12}$ (CSSO) garnet doped with

Special Issue: Phosphors for Infrared Applications

Received: January 17, 2023
Accepted: April 4, 2023

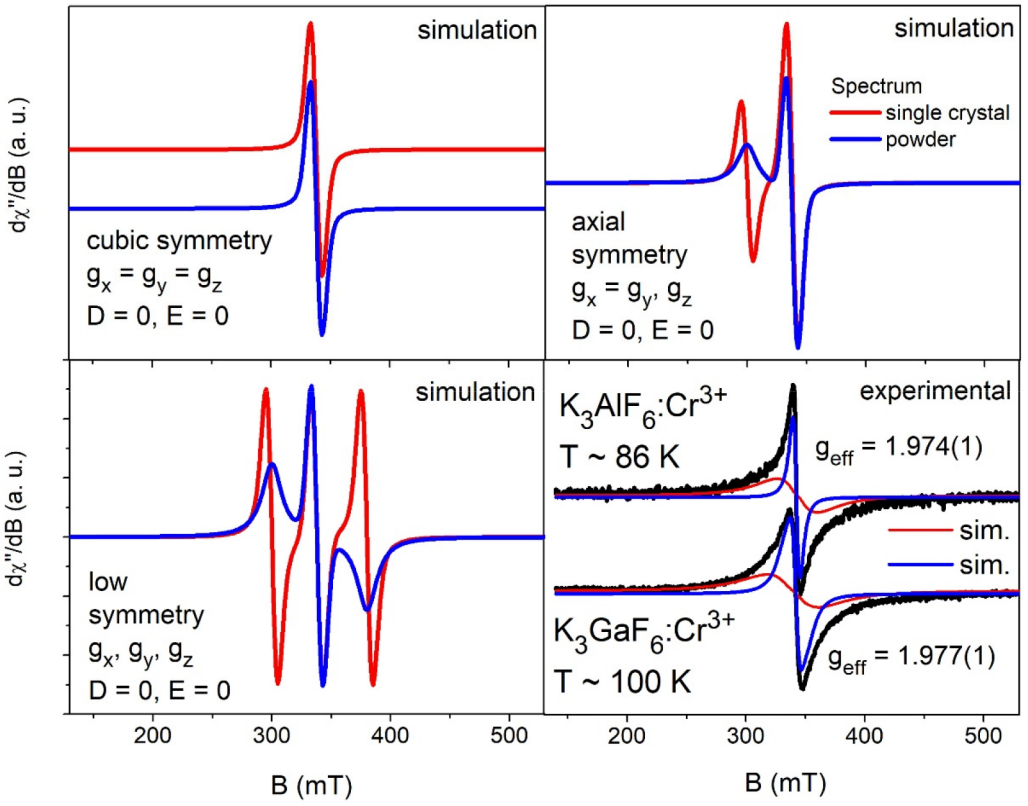

Figure 1. Simulated EPR spectra for compounds in the form of single crystals (red) and powders (blue) for magnetic ions with spin $S = 1/2$ for cubic symmetry (top left panel), axial symmetry (top right panel) and low symmetry (bottom left panel). Experimental (black) and simulated (red and blue) EPR spectra for cubic symmetry of Cr^{3+} ions in K_3AlF_6 and K_3GaF_6 compounds.[27]

Cr^{3+} ions. Optical studies show only one Cr^{3+} center in the octahedral site for the CSSO garnet synthesized under the air condition and in a CO reducing atmosphere. Diffuse reflection (DR) studies showed the occurrence of chromium ions in the fourth oxidation state under the air condition while sintering in a CO reducing atmosphere showed the absence of Cr^{4+} ions. The authors presented two EPR spectra, one each for the compound CSSO + Air and CSSO + CO. Two EPR lines were observed at $g_{eff} \sim 3.9$ and $g_{eff} \sim 2.0$. The line at $g_{eff} \sim 3.9$ was assigned as originating from single Cr^{3+} ions in the octahedral site, while the line at $g_{eff} \sim 2$ derived from $Cr^{3+}-Cr^{3+}$ pairs. The first EPR signal originates from single Cr^{3+} ions in an octahedral site. The second signal at $g_{eff} \sim 2$ is not from $Cr^{3+}-Cr^{3+}$ pairs. Its intensity is too low for this signal to be derived from pairs. For the compound CSSO + Air, its observe a weak symmetric signal at $g_{eff} = 2.00$. If this signal has a Lorentz shape, then the signal originates from defects in the crystal lattice associated with substitution of Cr^{4+} ions into sites of different valency. The second signal for the compound CSSO + CO at $g_{eff} = 1.99$ with observable shape asymmetry is only a component of the signal originating from single Cr^{3+} ions in octahedral site. To definitively prove the absence of $Cr^{3+}-Cr^{3+}$ ion pairs, temperature EPR studies should be performed to determine the temperature dependence of magnetic susceptibility. The signal from $Cr^{3+}-Cr^{3+}$ ion pairs for the CSSO:Cr^{3+} compound and confirmed by temperature studies of magnetic susceptibility is shown in Figure 4 (second panel from the top).

Very often in scientific papers on the luminescence of Cr^{3+} ions, the line at $g_{eff} \sim 2$ is attributed to $Cr^{3+}-Cr^{3+}$ pairs, while other studies do not show the existence of $Cr^{3+}-Cr^{3+}$ pairs. In the present paper, I present that the signal at $g_{eff} \sim 2$ may originate not only from Cr^{3+} ion pairs but also from defects in the crystal lattice or is only a component of the signal from single Cr^{3+} ions in an octahedral site. To definitively determine where the EPR line at $g_{eff} \sim 2$ originates, a temperature analysis of magnetic susceptibility should be performed.

EPR studies are easy for single ions with electron spin $S = 1/2$ but become more difficult when the material contains ions with higher electron spins, additional nuclear spins, several magnetic ions in incoherent lattice sites, strong magnetic interactions, or defects in the crystal lattice. It is also important to distinguish between the EPR signal from single crystals and powders (polycrystalline materials). The shape of the EPR spectrum from powder materials can differ significantly from the shape of the EPR spectrum from single crystals, as powder spectra are the sum of all the spectra from different orientations of the monocrystal with respect to the external magnetic field and microwave radiation.

This paper will present a structural analysis of the nearest environment of ions with $S = 3/2$ spin based on powder EPR spectra of luminescent chromium ions.

EXPERIMENTAL SECTION

The presented EPR spectra were recorded at room temperature using a conventional Bruker X-band ELEXSYS E500 CW spectrometer operating at 9.46 GHz. The magnetic induction was up to 1.4 T. The first derivative of the absorption spectrum was recorded as a function of the applied magnetic induction.

Simulations of the EPR spectra and fitting of the Spin Hamiltonian (SH) parameters to the experimental data were performed using EPR-NMR computer software.[34]

Magnetic measurements were performed with a SQUID (Superconducting QUantum Interference Device) magnetometer (Quantum

https://doi.org/10.1021/acsaom.3c00018
ACS Appl. Opt. Mater. XXXX, XXX, XXX−XXX

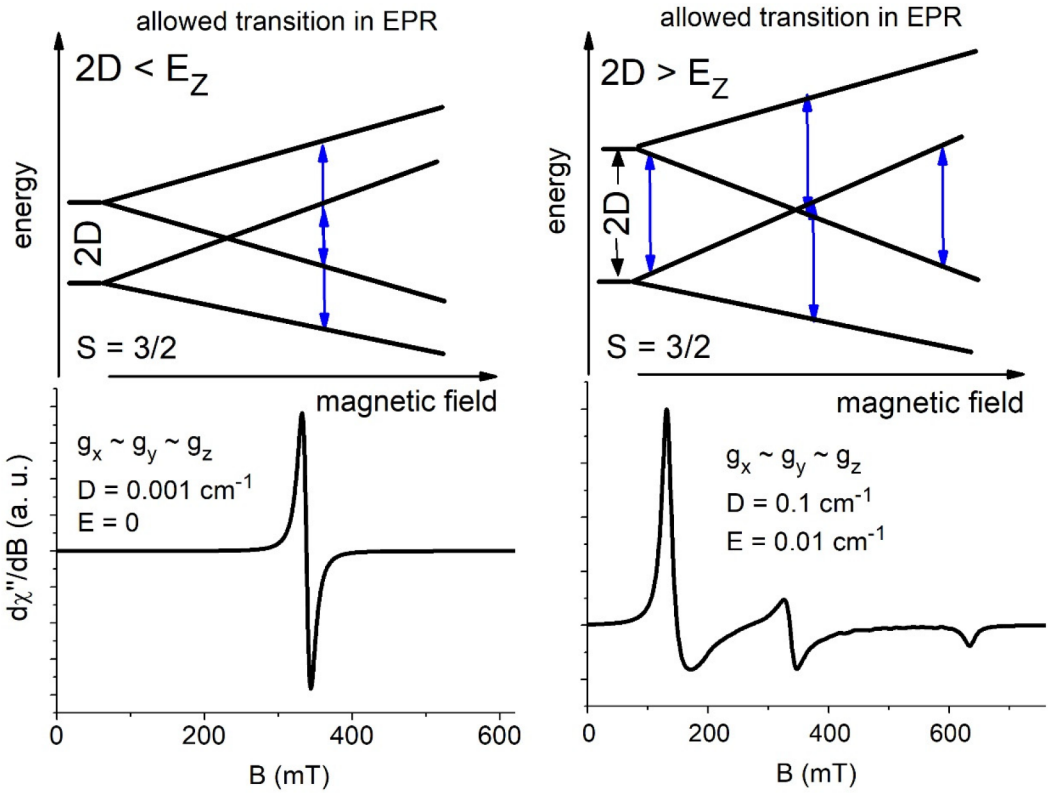

Figure 2. Simplified diagrams of low-lying energy levels for isolated ions with $S = 3/2$ spin (e.g., Cr^{3+}) for weak (top left panel) and strong (top right panel) crystal fields. The double-sided arrows represent possible EPR transitions. The lower panels show simulated EPR spectra corresponding to the above diagrams.

Design MPMS-XL-7). Measurements were recorded for temperatures up to 300 K with a magnetic field of $H = 1$ kOe. The susceptibility data were corrected for the diamagnetism of the sample holder and constituent atoms using Pascal's constants.[35]

RESULTS AND DISCUSSION

EPR research is based on the absorption of microwave radiation by unpaired electrons as a result of the splitting of the ground energy level under the influence of an external magnetic field (Zeeman effect). As a result of the resonance between the microwave energy and the difference in splitting energy between the lowest ground-state levels, the electron jumps to a level at higher energy. It remains at this level for a time called relaxation time, then decays to the ground state and emits radiation of energy equal to the difference between the excited and ground states. This radiation is recorded by a spectrometer. The shape of this signal can be Lorentzian, Gaussian, or a mixed one, called a Voigt curve, depending on magnetic interactions. Free ion spectra (without interactions) have a Lorentzian shape. EPR spectra are presented in the form of the first derivative of these curves to facilitate analysis of the peak-to-peak line width and the position of the resonance line as a function of magnetic induction. Unlike static magnetic susceptibility, which is determined from the difference in magnetic field strength (H) with and without a sample (e.g., magnetometer measurements), EPR studies report the value of magnetic induction (B) rather than the external magnetic field. The value of the magnetic induction at which magnetic resonance occurs strictly depends on the microwave frequency (for free ions). Typical spectrometers have a microwave range of $f \sim 9$ GHz (X-band), but there are also spectrometers with much higher microwave frequencies and higher external magnetic fields. To compare the results of spectrophotometers operating in different microwave frequency ranges, the position of the EPR line is determined by the formula $g_{eff} = 71.44773 f_{rez}(\mathrm{GHz})/B_{rez}(\mathrm{mT})$, where g_{eff} is the effective value read from the experimental data and should only apply to the main line for a single magnetic center. For a free ion with spin $S = 1/2$, the EPR signal will be observable at $g_{eff} = 2.0023$, any difference in signal position will be due to a variation in the nearest environment of the magnetic center.

The trivalent chromium ion Cr^{3+} has an electron configuration of $3d^3$. The ground state $^4A_2$ (4F; $L = 3$, $S = 3/2$) splits in a crystal field, so the lowest energy is associated with the ground state composed of two Kramer doublets (ms = $\pm 1/2$, $\pm 3/2$) which split under the influence of an external magnetic field. Transitions between the levels of the described quartet with the selection rule $\Delta ms = \pm 1$ are recorded in the EPR spectrum. No hyperfine interactions with nuclear spin $I = 3/2$ are observed in the EPR spectrum due to the low abundance (9.5%) of ^{156}Cr isotopes. Fine interactions with $S = 3/2$ spin are observed in the EPR spectrum.

Simulations of the EPR spectra and fitting of the Spin Hamiltonian (SH) parameters to the experimental data were performed using EPR-NMR computer software.[34]

Figure 1 shows simulations of EPR spectra for single crystals and powder materials performed with the EPR-NMR program for ions with spin $S = 3/2$. For cubic symmetry, it observes a single EPR line (top left panel) in superposition originating from unpaired electrons for both single crystals and powder compounds. For axial symmetry (upper right panel) and lower symmetry (lower left panel), EPR signal splitting is observed.

https://doi.org/10.1021/acsaom.3c00018
ACS Appl. Opt. Mater. XXXX, XXX, XXX−XXX

Chromium ions have low magnetic anisotropy ($g_x \sim g_y \sim g_z$), therefore the Zeeman splitting coefficients (g_x, g_y, g_z) have similar values and no fine interactions are observed and the splitting of the EPR spectrum derives from other effects. The low anisotropy of transition metal ions is due to the electron configuration. Unpaired electrons occur on the 3d shell and are not shielded from external conditions as is the case for rare earth. This removes the primary degeneracy of the orbital level ($L = 0$) with a strong crystal field of high symmetry which leads to the low anisotropy of transition metal ions. The EPR spectra presented in Figure 1 (upper right and lower left panels) are observed for ions with spin $S = 3/2$ and high magnetic anisotropy, such as RE^{3+} ions in less than cubic symmetry. Figure 1 (lower right panel) shows EPR spectra for K_3AlF_6:0.03Cr^{3+} and K_3GaF_6:0.03Cr^{3+} compounds in which Cr^{3+} ions occupy the cubic symmetry site (blue curve). The fit of the Voigt curve to the experimental data indicates at least two magnetic centers. The second magnetic center (of much lower intensity) is located in a lower than cubic symmetry (red curve). Both Cr^{3+} centers were confirmed by optical studies.[27]

In an octahedral crystal field, the ground state splits into two Kramers doublets separated by $2D$, where D is the zero-field splitting parameter.

Figure 2 shows energy diagrams for ions with $S = 3/2$ spin (e.g., Cr^{3+}) for weak ($2D < E_z$ (E_z is Zeeman energy) and strong ($2D > E_z$) crystal fields. The lower panels of Figure 2 show the EPR spectra corresponding to the above diagrams. These are simulations of EPR spectra performed with the EPR-NMR program for isolated chromium ions ($g_x \sim g_y \sim g_z$, $D > 0$). The intensity of the EPR line (intensity as amplitude) indicates the probability of transition between energy levels. EPR transitions occur between energy levels $\leftarrow 1/2||1/2\rangle$, $\leftarrow 3/2||3/2\rangle$ and $\langle 1/2||-3/2\rangle$, $\leftarrow 3/2||1/2\rangle$. The first ones depend on the anisotropy of the magnetic ion (g_x, g_y, g_z) while the second ones depend on the crystal field (D). The positions of the EPR transitions in magnetic induction for transition metal ions with low symmetry strongly depend on the crystal field (D-values).

Figure 3 shows simulations of EPR spectra for Cr^{3+} ions with spin $S = 3/2$ for different values of the ZFS parameters $D > 0$, $E = 0$ (E is the second ZFS parameter for low site symmetries), and $D \gg 0$, $E = 0$ (left panel) and $D > 0$, $E \neq 0$ and $D \gg 0$, $E \neq 0$ (right panel). Simulations show that as D and E increase, the EPR spectrum splits and several EPR lines in a wide range of magnetic induction can belong to one magnetic center (e.g., Cr^{3+}). Depending on the magnitude of D and E, EPR lines can be observed even above $B > 800$ mT. The magnitudes D and E are strongly related to the nearest environment of the magnetic ion (Cr^{3+}) and the magnitude D represents the axial distortion, while E represents the rhombic distortion of the nearest environment of the magnetic ion. For the values to be correct, the relation $0 \leq E/D \leq 1/3$ must be fulfilled. It is worth noting (Figure 3, right panel, EPR signal marked with a red curve) for large axial distortions of the nearest environment of the Cr^{3+} ion, it is observed an EPR line at $g_{eff} \sim 2$ which is a component of the EPR signal originating from an isolated center in a highly distorted octahedral environment. In many scientific publications, optical studies indicate the presence of only one luminescent center, while in the EPR spectra, in addition to the signal at low magnetic inductions ($g_{eff} \sim 4-5$), an additional signal is observed at $g_{eff} \sim 2$. According to the simulations, this is a component of the signal originating from isolated Cr^{3+} ions in an octahedral environment with high distortion, not an additional Cr^{3+} center.

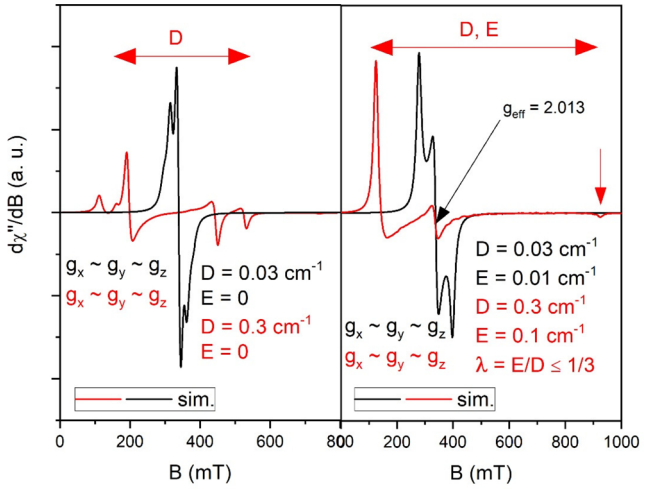

Figure 3. Simulated EPR spectra obtained with EPR-NMR software for different values of the ZFS parameters (D, E value).

In the case of luminescent materials based on Cr^{3+} ions at $g_{eff} \sim 2$, EPR lines originating from $Cr^{3+}-Cr^{3+}$ ion pairs, crystal lattice defects (e.g., in the form of lattice vacancies and localized electrons), and conduction electrons can be observed in addition to luminescent centers at highly distorted octahedral sites. The conduction electrons are easily recognized due to the Dyson shape of the EPR line and the broad EPR line width. Crystal lattice defects and $Cr^{3+}-Cr^{3+}$ ion pairs are somewhat more difficult to recognize, both of which can be intense (with large signal amplitude) and very narrow, the only difference being minor shifts in line position relative to magnetic induction. Signals from $Cr^{3+}-Cr^{3+}$ ion pairs are below the value of 2, i.e., $g_{eff} \sim 1.96-1.99$, while signals from crystal lattice defects (with $S = 1/2$ spin, e.g., electrons trapped in vacancies of the crystal lattice) are located at $g_{eff} = 2.00023$.

Figure 4 shows luminescent materials based on Cr^{3+} ions. In all spectra, there is an EPR signal at $g_{eff} \sim 2$. For the first two compounds (first and second panels from the top), the EPR signal originates from $Cr^{3+}-Cr^{3+}$ ion pairs and was confirmed by temperature EPR and static magnetic susceptibility SQUID studies. For the third compound (panel third from top), the EPR signal is derived from crystal lattice defects with the spin $S = 1/2$ as electrons trapped in the vacancies of the crystal lattice. Temperature EPR and SQUID studies did not reveal the presence of pair interactions in the investigated compound. For the last compound (lower panel), a broad signal from free electrons is observed. Temperature EPR studies indicate that electrons transfer into the conduction band as a result of the thermal vibrations of the material.

An important result of EPR studies is the determination of the point symmetry of the nearest environment of the luminescent (magnetic) ion. The symmetry of the nearest environment of the magnetic ion is determined by fitting the spin Hamiltonian (SH) parameters to the experimental data. The spin Hamiltonian should include all interactions observed on the EPR spectrum. For Cr^{3+} ions with spin $S = 3/2$, the SH should contain the terms: Zeeman (H_Z), Zero-field splitting (H_{ZFS}), and pair interaction (H_{pair}) if present. The complete SH is as follows:

https://doi.org/10.1021/acsaom.3c00018
ACS Appl. Opt. Mater. XXXX, XXX, XXX−XXX

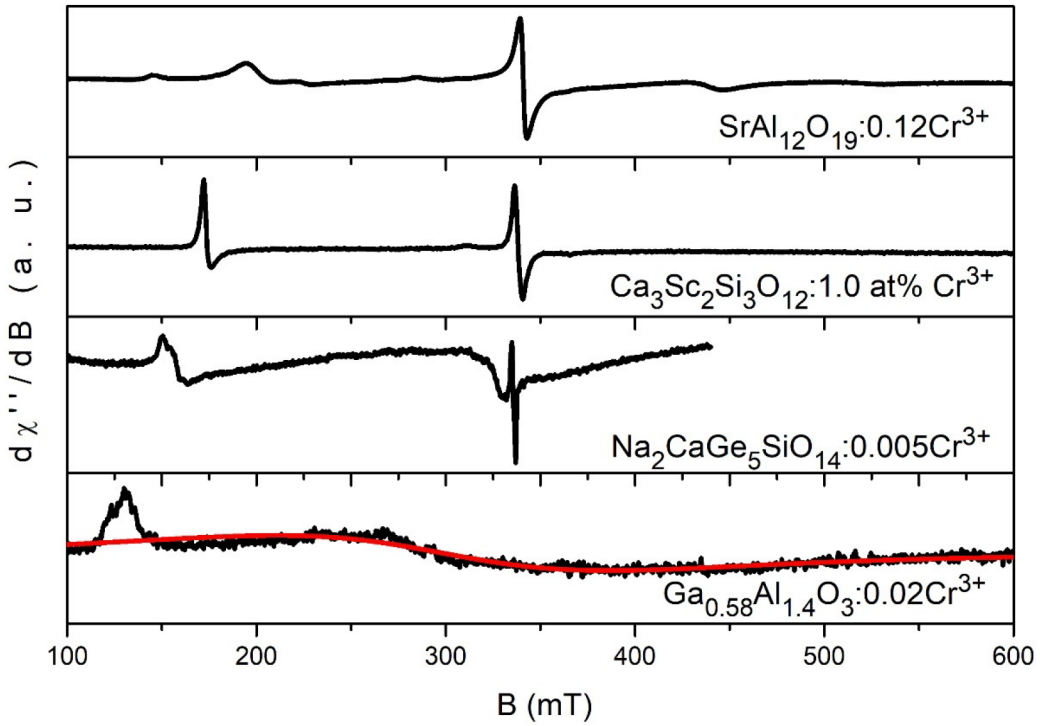

Figure 4. Four experimental EPR spectra for $SrAl_{12}O_{19}$,[19] $Ca_3Sc_2Si_3O_{12}$, $Na_2CaGe_5SiO_{14}$, and $Ga_{0.58}Al_{1.4}O_3$[22] compounds doped with Cr^{3+} ions at different concentrations. The red line shows the fit of the Dyson line for the conduction electrons.

$$H = H_Z + H_{ZFS} + H_{pair} = \mu_B g\mathbf{BS} + D\left(S_z^2 - \frac{1}{3}S(S+1)\right) + E(S_x^2 + S_y^2) + \mathbf{S}^A\mathbf{D}\mathbf{S}^B \quad (1)$$

$$H_Z = \mu_B g\mathbf{BS} = \mu_B(g_x B_x S_x + g_y B_y S_{xy} + g_z B_z S_z) \quad (2)$$

where μ_B is Bohr magneton, **B** is induction of magnetic field, g is spectroscopic splitting factor (g, g_x, g_y, $g_z \neq g_{eff}$); **S**, $\mathbf{S}^A$, and $\mathbf{S}^B$ are electron spin; D and E are axial and rhombic distortions of octahedral, and **D** is the general matrix of interactions, respectively. For powder compounds with S = 3/2 spin, one of three point symmetries can be specified: low, axial, or cubic. For the highest (cubic) symmetry based on the fit, the SH parameters should have the values: $g_x = g_y = g_z = g$, $D = 0$, $E = 0$, while for the axial symmetry: $g_x = g_y \neq g_z$, $D \neq 0$, $E = 0$, for the lowest symmetry: $g_x \neq g_y \neq g_z$, $D \neq 0$, $E \neq 0$. An example EPR spectrum of Cr^{3+} ions for cubic symmetry is shown in Figure 1 (top left panel), for axial symmetry in Figure 3 (left panel), and low symmetry in Figure 3 (right panel).

The temperature dependence of the EPR magnetic susceptibility makes it possible to determine the nature and strength of the interactions between magnetic ions. The strength of the interactions between the ions is a direct result of the structure of the compound. Isolated luminescent ions have a higher luminescence efficiency, due to energy dissipation by interion interactions. On the other hand, energy transfer between dissimilar ions will be most efficient if the distances between ions are as small as possible. These data can only be obtained from investigations using the EPR technique, which gives the actual interactions between luminescent ions (even small amounts of dopants), while other techniques give the distances between the host ions of a compound and not the introduced dopants. To know the strength of the interactions between the magnetic ions, the temperature characteristics of the magnetic susceptibility EPR must be determined. The characteristics of free ions are described by Curie's law and those of interacting magnetic ions by Curie–Weiss law:

$$\chi_{EPR} = \frac{C_{EPR}}{T - T_{CW}} \quad (3)$$

$$\chi_{SQUID} = \frac{C_{SQUID}}{T - T_{CW}} \quad (4)$$

where T_{CW} is the Curie–Weiss temperature, C_{EPR} a constant, and C_{SQUID} the Curie constant determined from static magnetic susceptibility with a magnetometer. The value and sign of the Curie–Weiss temperature indicate the strength and nature of the magnetic interactions between the ions. Negative T_{CW} values indicate antiferromagnetic interactions, while positive values indicate ferromagnetic interactions. The strength of the interactions is determined by the T_{CW} magnitude. With a magnetometer, it is also possible to determine the Curie constant from which the effective magnetic moment can be determined ($\mu_{eff} = 2.827\sqrt{C}\mu_B$). This gives information on the valence of the magnetic ions involved in the magnetic susceptibility of the material being investigated. Also, the type of magnetic ions or, in the case of a larger number of dissimilar magnetic ions, the concentration of these ions in the material.

In the case of pair interactions of magnetic ions, the temperature dependence of magnetic susceptibility behaves according to the Bleaney–Bowers equation:

$$\chi = \frac{C_1}{T}\frac{1}{1 + (1/3)\exp(-2J/kT)} \quad (5)$$

https://doi.org/10.1021/acsaom.3c00018
ACS Appl. Opt. Mater. XXXX, XXX, XXX−XXX

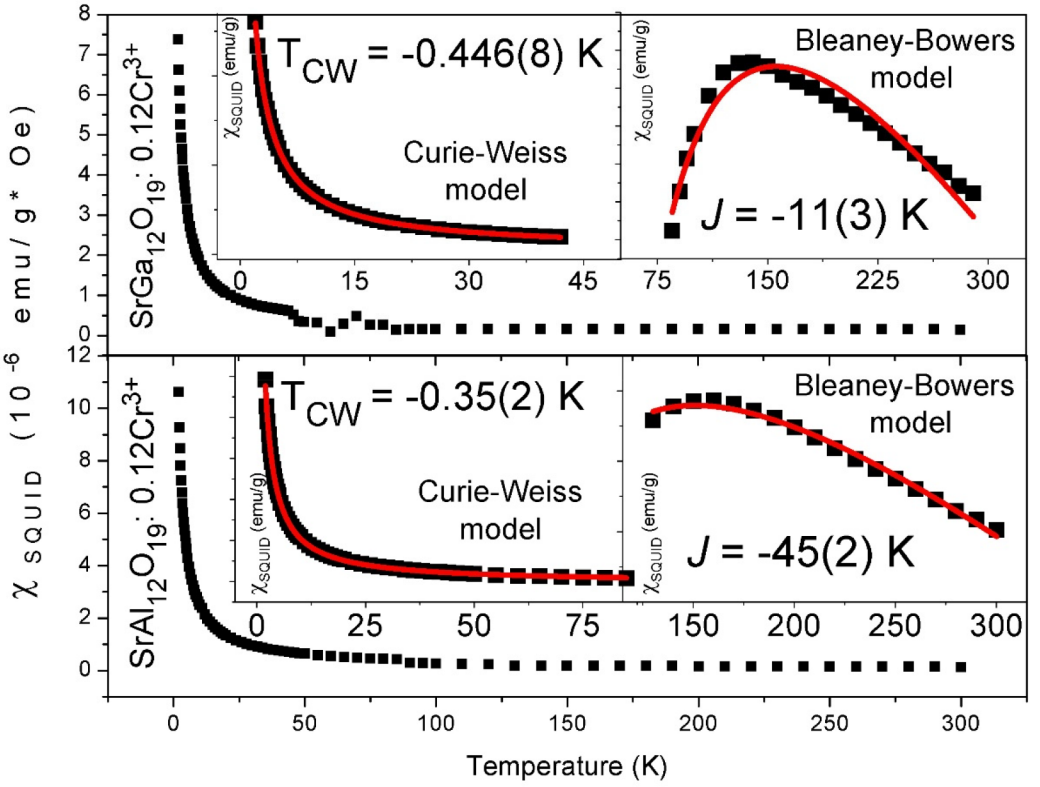

Figure 5. Static magnetic susceptibility for two compounds $SrGa_{12}O_{19}$ (upper panel) and $SrAl_{12}O_{19}$ (lower panel) doped with Cr^{3+} ions over the full temperature range from 2 K. Insets, Curie−Weiss equation fit to experimental data (left panels) and Bleaney−Bowers fit (right panels).[19]

where the notations have standard meanings and J is the exchange interaction constant.

Depending on the type of ion to be investigated, an appropriate range of temperature measurements should be selected. Due to the nonzero orbital moment ($L \neq 0$), EPR spectra of rare earth ions are observed at helium temperatures in the range up to about 40 K. Transition metal ions, whose orbital moment is quenched ($L = 0$), can be investigated in the full range of temperature up to room temperature. Cr^{3+} ions can be investigated in the full temperature range, but it must be considered that the Curie−Weiss law (eq 4) and the Bleaney−Bowers law (eq 5) are only fulfilled for nonlarge magnetic fields and temperatures above the Curie temperature. The equation $H/kT \ll 1$ must be fulfilled. Isolated Cr^{3+} ions at octahedral sites have a low T_{CW} value of up to a few Kelvin degrees, so the measuring range should be close to the T_{CW} temperature. Therefore, temperature studies of magnetic susceptibility for Cr^{3+} ions should be performed over the full temperature range. Exemplary CW + BB characteristics of magnetic susceptibility behavior over the full temperature range for two compounds $SrAl_{12}O_{19}$:0.012Cr^{3+} and $SrGa_{12}O_{19}$:0.012Cr^{3+} are shown in Figure 5.

The EPR signal at $g_{eff} \sim 2$ does not always originate from Cr^{3+}−Cr^{3+} ions; to definitively confirm or deny the existence of pairs, magnetic susceptibility studies must be performed over the full temperature range. For the $SrAl_{12}O_{19}$:0.12Cr^{3+} compound, the EPR spectrum is presented in Figure 4 (first panel from the top). The signal at $g_{eff} = 1.98$ is narrow, symmetrical and intense, so it can be assumed to originate from Cr^{3+} ion pairs. Confirmation of the existence of the pairs has been provided by temperature studies of magnetic susceptibility with the SQUID magnetometer (Figure 5). At low temperatures (Figure 5, upper panel, left inset), the characteristics are described by the CW law (eq 4), which indicates that there are single Cr^{3+} ions with small antiferromagnetic interactions in the sample. At higher temperatures (Figure 5, upper panel, right inset), the characteristics are described by the BB eq 5, which indicates the presence of Cr^{3+}−Cr^{3+} ion pairs. Temperature studies of magnetic susceptibility confirm that the EPR signal at $g_{eff} = 1.98$ comes from Cr^{3+}−Cr^{3+} ion pairs. For the $SrGa_{12}O_{19}$:0.12Cr^{3+} compound, the EPR spectrum is shown in Figure 6. The EPR signal from Cr^{3+}−Cr^{3+} ion pairs is almost invisible in the background of the signal from single Cr^{3+} ions in

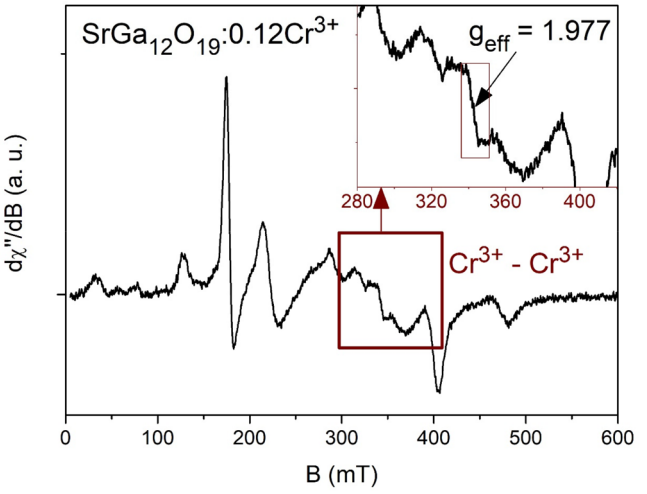

Figure 6. Experimental EPR spectrum of the $SrAl_{12}O_{19}$:0.12Cr^{3+} compound.[19]

https://doi.org/10.1021/acsaom.3c00018
ACS Appl. Opt. Mater. XXXX, XXX, XXX−XXX

an octahedral environment. EPR studies at only one temperature will not reveal the presence of Cr^{3+}−Cr^{3+} ion pairs, to have confirmation of the presence of Cr^{3+} pairs one has to perform temperature studies of magnetic susceptibility. If the magnetic susceptibility in a certain temperature range can be described by the BB equation it confirms the existence of magnetic ion pairs. For the $SrGa_{12}O_{19}$:0.12Cr^{3+} compound, the magnetic susceptibility characteristics described by the CW law (eq 4) were observed at low temperatures (Figure 5, bottom panel, left inset) and those described by the BB eq 5 at higher temperatures (Figure 5, bottom panel, right inset). This indicates that Cr^{3+} ions are present in two different configurations in the studied material. As single Cr^{3+} ions in an octahedral setting with weak antiferromagnetic interactions and Cr^{3+}−Cr^{3+} ion pairs with weak antiferromagnetic interactions.

CONCLUSIONS

Electron paramagnetic resonance (EPR) magnetic studies make it possible to determine the nearest environment of luminescent ions if these ions have unpaired electrons (magnetic ions). The position of the EPR line (g_{eff}) makes it possible to determine the magnetic (luminescent) center and its environment. In luminescent materials doped with Cr^{3+} ions, one can distinguish isolated Cr^{3+} ions in an octahedral site, Cr^{3+}−Cr^{3+} ion pairs, crystal lattice defects, and conduction electrons. Diamagnetic ions do not provide an EPR signal, but also influence the nearest environment of luminescent ions causing, for example, an increase in luminescence efficiency and, in magnetic studies, variations in the spin Hamiltonian parameters. Therefore, the effect of diamagnetic ions on the nearest environment of magnetic (luminescent) ions can be investigated using the EPR technique. From the parameters of the spin Hamiltonian, the point symmetry and distortion of the nearest environment of the luminescent ion can be determined. This is one of the most important elements as it influences the position and shape of the luminescence spectrum. Temperature EPR studies make it possible to determine the nature and strength of the interactions between magnetic (luminescent) ions, which influence luminescence efficiency. In addition, static magnetic susceptibility investigations make it possible to determine the valence and/or concentration of magnetic ions in the investigated material.

EPR studies are the only technique that investigates the nearest environment of the doped luminescent ions and not the host ions. Therefore, to determine the nearest environment of luminescent ions, the EPR technique is essential.

AUTHOR INFORMATION

Corresponding Author

Grzegorz Leniec − *Department of Technical Physics, Faculty of Mechanical Engineering and Mechatronics, West Pomeranian University of Technology in Szczecin, Szczecin 70-310, Poland;* orcid.org/0000-0002-7980-6992; Email: gleniec@zut.edu.pl

Complete contact information is available at: https://pubs.acs.org/10.1021/acsaom.3c00018

Notes

The author declares no competing financial interest.

REFERENCES

(1) Dave, K.; Huang, W.-T.; Leśniewski, T.; Lazarowska, A.; Grzegorczyk, M.; Mahlik, S.; Leniec, G.; Kaczmarek, S. M.; Liu, R.-S. Enhancement of self-trapped excitons and near-infrared emission in Bi^{3+}/Er^{3+} co-doped $Cs_2Ag_{0.4}Na_{0.6}InCl_6$ double perovskite. *Nanoscale* **2022**, *14*, 17735−17742.

(2) Zając, A.; Solarz, P.; Ptak, M.; Lorenc, J.; Kaczmarek, S. M.; Leniec, G.; Hermanowicz, K.; Hanuza, J. Synthesis, optical and magnetic studies of cerium and europium phytate complexes -new microporous materials. *J. Mol. Struct.* **2021**, *1233*, 130114.

(3) Pilarek, B.; Ptak, M.; Hanuza, J.; Szczygieł, I.; Leniec, G.; Kaczmarek, S. M. Structural, vibrational and magnetic properties of high-temperature $(Ca_4Nb_2)_{1-x}Nd_{2x}O_{9-6x}$ solid solution. *J. Solid State Chem.* **2021**, *304*, 122620.

(4) Leniec, G.; Kaczmarek, S. M.; Macalik, L.; Ropuszyńska-Robak, P.; Hanuza, J. Magnetic properties of $KY_{0.93}Er_{0.05}Tm_{0.02}(WO_4)_2$ and $NaY_{0.97}Er_{0.02}Tm_{0.01}(WO_{4)2}$ nanocrystals obtained using Pechini and hydrothermal methods. *J. Phys. Chem. Solids* **2020**, *138*, 109273.

(5) Kaczmarek, S. M.; Witkowski, M. E.; Głowacki, M.; Leniec, G.; Berkowski, M.; Kowalski, Z. W.; Makowski, M.; Drozdowski, W. $BaWO_4$: Pr single crystals co-doped with Na. *J. Cryst. Growth* **2019**, *528*, 125264.

(6) Godlewska, p.; Macalik, L.; Lorenc, J.; Lisiecki, R.; Ryba-Romanowski, W.; Hanuza, J.; Kaczmarek, S. M.; Fuks, H.; Leniec, G. Optical and magnetic properties of neodymium(III) six-coordinate complexes of 2,6-lutidine N-oxide derivatives. *J. Solid State Chem.* **2019**, *276*, 294−301.

(7) Leniec, G.; Kaczmarek, S. M.; Bodziony, T.; Fuks, H.; Kowalski, Z.; Berkowski, M.; Głowacki, M. Site Symmetries of Cerium Ions in $BaWO_4$ Single Crystals Codoped with Sodium Ions. *Appl. Magn. Reson.* **2019**, *50* (6), 819−833.

(8) Leniec, G.; Kaczmarek, S. M.; Macalik, L.; Ropuszyńska-Robak, P.; Hanuza, J. Magnetic properties of $NaY_{1-x-y}Ho_xYb_y(WO_4)_2$: x = 0.05, y = 0.02 and $KY_{1-x-y}Ho_xYb_y(WO_4)_2$: x = 0.02, y = 0.01 nanopowders obtained by Pechini and hydrothermal methods. *Chem. Phys. Lett.* **2019**, *715*, 360−366.

(9) Kaczmarek, S. M.; Leniec, G.; Fuks, H.; Skibiński, T.; Pelczarska, A.; Godlewska, P.; Hanuza, J.; Szczygieł, I. Magnetic properties of $Na_3Ln(PO_4)_2$ orthophosphates codoped with erbium and chromium (Ln = La, Gd)". *Materials Science-Poland* **2017**, *35* (4), 733−745.

(10) Kaczmarek, S. M.; Leniec, G.; Fuks, H.; Skibiński, T.; Pelczarska, S.; Godlewska, P.; Hanuza, J.; Szczygieł, I. Magnetic Investigations of Microcrystalline $Na_3Ln_{0.99-x}Er_{0.01}Cr_x(PO_4)_2$ Orthophosphates Synthesized by Pechini Method (Ln = La, Gd). *World Journal of Applied Physics* **2017**, *2* (1), 7−18.

(11) Kaczmarek, S. M.; Leniec, G.; Berkowski, M.; Kazan, S.; Acikgoz, M. Magnetic properties of $La_3Ga_{5.5}Ta_{0.5}O_{14}$ single crystals doped with Sm^{3+} and Er^{3+} ions. *Acta Phys. Polym., A* **2017**, *131* (3), 366−369.

(12) Leniec, G.; Kaczmarek, S. M.; Berkowski, M.; Acikgoz, M.; Kazan, S. Investigations on magnetic properties of $La_3Ga_{5.5}Ta_{0.5}O_{14}$ single crystals doped with Er^{3+} ions. *J. Alloys Compd.* **2017**, *699*, 11−15.

(13) Kaczmarek, S. M.; Leniec, G.; Skibiński, T.; Pelczarska, A.; Szczygieł, I.; Hanuza, J. EPR and magnetic studies of sub-microcrystalline pure and Yb doped $Na_3Gd(PO_4)_2$ orthophosphates synthesized by hydrothermal and Pechini method. *Science Advances Today* **2016**, *2*, 25243.

(14) Kaczmarek, S. M.; Leniec, G.; Berkowski, M.; Acikgoz, M.; Kazan, S. Magnetic properties of $La_3Ga_{5.5}Ta_{0.5}O_{14}$ single crystals doped with Sm^{3+}. *J. Alloys Compd.* **2016**, *687*, 696−700.

(15) Leniec, G.; Kaczmarek, S. M.; Berkowski, M.; Głowacki, M.; Skibiński, T.; Bojanowski, B. Growth and EPR properties of $ErVO_4$ single crystals. *Nukleonika* **2015**, *60* (3), 405−410.

(16) Chang, C.-Y.; Majewska, N.; Chen, K.-C.; Huang, W.-T.; Leśniewski, T.; Leniec, G.; Kaczmarek, S. M.; Pang, w. K.; Peterson, V. K.; Cherng, D.-H.; Lu, K.-M.; Mahlik, S.; Liu, R.-S. Broadening Phosphor-Converted Light-Emitting Diode Emission: Controlling Disorder. *Chem. Mater.* **2022**, *34* (22), 10190−10199.

(17) Chen, Y.; Bao, Z.; Huang, W.; Lazarowska, A.; Majewska, N.; Mahlik, S.; Leniec, G.; Kaczmarek, S. M.; Huang, H.; Wu, C.; Huang,

D.; Liu, R.-S. Effect of Temperature and Pressure on Structural and Optical Properties of Organic−Inorganic Hybrid Manganese Halides. *Inorg. Chem.* **2022**, *61* (5), 2595−2602.
(18) Yuan, C.; Li, R.; Liu, Y.; Zhang, L.; Zhang, J.; Leniec, g.; Sun, P.; Liu, Z.; Luo, Z.; Dong, R.; Jiang, J. Efficient and Broadband $LiGaP_2O_7:Cr^{3+}$ Phosphors for Smart Near-Infrared Light-Emitting Diodes. *Laser & Photonics Reviews* **2021**, *15*, 2100227.
(19) Rajendran, V.; Fang, M.-H.; Huang, W.-T.; Majewska, N.; Lesniewski, T.; Mahlik, S.; Leniec, G.; Kaczmarek, S. M.; Pang, W. K.; Peterson, V. K.; Lu, K.-M.; Chang, H.; Liu, R.-S. Chromium Ion Pair Luminescence: A Strategy in Broadband Near-Infrared Light-Emitting Diode Design. *J. Am. Chem. Soc.* **2021**, *143* (45), 19058−19066.
(20) Fang, M.-H.; Chen, K.-C.; Majewska, N.; Leśniewski, T.; Mahlik, S.; Leniec, G.; Kaczmarek, S. M.; Yang, C.-W.; Lu, K.-M.; Sheu, H.-S.; Liu, R.-S. Hidden Structural Evolution and Bond Valence Control in Near-Infrared Phosphors for Light-Emitting Diodes. *ACS Energy Letters* **2021**, *6* (1), 109−114.
(21) Li, R.; Liu, Y.; Yuan, C.; Leniec, G.; Miao, L.; Sun, P.; Liu, Z.; Luo, Z.; Dong, R.; Jiang, J. Thermally Stable $CaLu_2Mg_2Si_3O_{12}:Cr^{3+}$ Phosphors for NIR LEDs. *Advanced Optical Materials* **2021**, *9*, 2100388.
(22) Chen, K.-C.; Fang, M.-H.; Huang, W.-T.; Kamiński, M.; Majewska, N.; Leśniewski, T.; Mahlik, S.; Leniec, G.; Kaczmarek, S. M.; Yang, C.-W.; Lu, K.-M.; Sheu, H.-S.; Liu, R.-S. Chemical and Mechanical Pressure-Induced Photoluminescence Tuning via Structural Evolution and Hydrostatic Pressure. *Chem. Mater.* **2021**, *33* (10), 3832−3840.
(23) Fang, M.-H.; Li, T.-Y.; Huang, W.-T.; Cheng, C.-L.; Bao, Z.; Majewska, N.; Mahlik, S.; Yang, C.-W.; Lu, K.-M.; Leniec, G.; Kaczmarek, S. M.; Sheu, H.-S.; Liu, R.-S. Surface-Protected High-Efficiency Nanophosphors via Space-Limited Ship-in-a-Bottle Synthesis for Broadband Near-Infrared Mini-Light-Emitting Diodes. *ACS Energy Letters* **2021**, *6* (2), 659−664.
(24) Fang, M.-H.; De Guzman, G. N. A.; Bao, Z.; Majewska, N.; Mahlik, S.; Grinberg, M.; Leniec, G.; Kaczmarek, S. M.; Yang, C.-W.; Lu, K.-M.; Sheu, H.-S.; Hu, S.-F.; Liu, R.-S. Ultra-high-efficiency near-infrared $Ga_2O_3:Cr^{3+}$ phosphor and controlling of phytochrome. *Journal of Materials Chemistry C* **2020**, *8*, 11013−11017.
(25) De Guzman, G. N. A.; Rajendran, V.; Bao, Z.; Fang, M.-H.; Pang, W.-K.; Mahlik, S.; Lesniewski, T.; Grinberg, M.; Molokeev, M. S.; Leniec, G.; et al. Multi-Site Cation Control of Ultra-Broadband Near-Infrared Phosphors for Application in Light-Emitting Diodes. *Inorg. Chem.* **2020**, *59* (20), 15101−15110.
(26) Fang, M.-H.; Huang, P.-Y.; Bao, Z.; Majewska, N.; Lesniewski, T.; Mahlik, S.; Grinberg, M.; Leniec, G.; Kaczmarek, S. M.; Yang, C.-W.; Lu, K.-M.; Sheu, H.-S.; Liu, R.-S. Penetration in Biological Tissue Using Light-Emitting Diodes with Highly Efficient Near-Infrared $ScBO_3:Cr^{3+}$ Phosphors. *Chem. Mater.* **2020**, *32* (5), 2166−2171.
(27) Lee, C.; Bao, Z.; Fang, M.-H.; Lesniewski, T.; Mahlik, S.; Grinberg, M.; Leniec, G.; Kaczmarek, S. M.; Brik, M. G.; Tsai, Y.-T.; Tsai, T.-L.; Liu, R.-S. Chromium(III)-Doped Fluoride Phosphors with Broadband Infrared Emission for Light-Emitting Diodes. *Inorg. Chem.* **2020**, *59* (1), 376−385.
(28) Rajendran, V.; Lesniewski, T.; Mahlik, S.; Grinberg, M.; Leniec, G.; Kaczmarek, S. M.; Pang, W.-K.; Lin, Y.-S.; Lu, K.-M.; Lin, C.-M.; Chang, H.; Hu, S.-F.; Liu, R.-S. Ultra-Broadband Phosphors Converted Near-Infrared Light Emitting Diode with Efficient Radiant Power for Spectroscopy Applications. *ACS Photonics* **2019**, *6* (12), 3215−3224.
(29) Rajendran, V.; Fang, M.-H.; De Guzman, G. N. A.; Lesniewski, T.; Mahlik, S.; Grinberg, M.; Leniec, G.; Kaczmarek, S. M.; Lin, Y.-S.; Lu, K.-M.; et al. Super Broadband Near-Infrared Phosphors with High Radiant Flux as Future Light Sources for Spectroscopy Applications. *ACS Energy Letters* **2018**, *3*, 2679−2684.
(30) Fang, M.-H.; Wu, W.-L.; Jin, Y.; Lesniewski, T.; Mahlik, S.; Grinberg, M.; Brik, M. G.; Srivastava, A. M.; Chiang, C.-Y.; Zhou, W.; Jeong, D.; Kim, S.-H.; Leniec, G.; Kaczmarek, S. M.; Sheu, H.-S.; Liu, R.-S. Control of Luminescence via Tuning of Crystal Symmetry and Local Structure in Mn^{4+}-Activated Narrow Band Fluoride Phosphors. *Angew. Chem.* **2018**, *130* (7), 1815−1819.
(31) Kaczmarek, S. M.; Tsuboi, T.; Leniec, A.; Nakai, Y.; Leniec, G.; Berkowski, M.; Huang, W. Temperature dependence of PL and EPR spectra of $Sr_{0.33}Ba_{0.67}Nb_2O_6$:Cr (0.02 mol %) single crystals. *J. Cryst. Growth* **2014**, *401*, 798−801.
(32) Fuks, H.; Skibiński, T.; Kaczmarek, S. M.; Hanuza, J.; Leniec, G.; Hermanowicz, K.; Mączka, M.; Ptak, M. Structural and optical properties of crystalline and nanocrystalline $NaIn(WO_4)_2:Cr^{3+}$. *J. Alloys Compd.* **2014**, *585*, 722−728.
(33) Jia, Z.; Yuan, C.; Liu, Y.; Wang, X.-Y.; Sun, P.; Wang, L.; Jiang, H.; Jiang, J. Strategies to approach high performance in Cr^{3+}-doped phosphors for high-power NIR-LED light sources. *Light: Science & Applications* **2020**, *9*, 86.
(34) Mombourquette, M. J.; Weil, J. A.; McGavi, D. G. *EPR-NMR User's Manual*; , Department of Chemistry, University of Saskatchewan: Saskatoon, SK, Canada, 1999.
(35) Bain, G. A.; Berry, J. F. Diamagnetic Corrections and Pascal's Constants. *J. Chem. Educ.* **2008**, *85* (4), 532−536.

https://doi.org/10.1021/acsaom.3c00018
ACS Appl. Opt. Mater. XXXX, XXX, XXX−XXX